Journal of Power Sources 196 (2011) 1222–1228

Contents lists available at ScienceDirect

Journal of Power Sources

journal homepage: www.elsevier.com/locate/jpowsour

Multi-objective topology optimization of end plates of proton exchange membrane fuel cell stacks

P. Lin, P. Zhou, C.W. Wu*

State Key Lab of Structural Analysis for Industrial Equipment, Faculty of Vehicle Engineering and Mechanics, Dalian University of Technology, Dalian 116024, Liaoning, China

ARTICLE INFO

Article history:
Received 9 July 2010
Received in revised form 26 August 2010
Accepted 26 August 2010

Keywords:
End plate
Topology optimization
Multi-objective

ABSTRACT

End plates of the proton exchange membrane fuel cell (PEMFC) need to be well designed because their strength and rigidity directly affect the clamping pressure distribution and thus affect the performance and lifetime of fuel cell stacks. In this paper, a multi-objective topology optimization model of the end plates in a PEMFC stack with nonlinear contact boundary conditions was established to obtain an optimized structural design. It was found that the design improved with topology optimization is not only light but also meets manufacturability requirements. This provides good guidance for the design of a high-performance end plate.

1. Introduction

The proton exchange membrane fuel cell (PEMFC) has attracted much attention as a promising power source with wide application owing to its high power efficiency, high energy density, quick cold-start capability and low level of pollution [1–4]. It is a possible substitute for combustion engines in automobiles and heat generators in houses. For PEMFCs to meet the requirements of practical applications, their performance and lifetime need to be optimized.

As the voltage and total power generated by a single PEMFC is rather limited, PEMFC products for practical applications comprise numerous planar single cells in series that form large stack structures with a cyclic cell characteristic. Typically, two end plates, between which the unit cells are inserted, are located on the outside of the stack to provide proper internal compression, and the entire fuel cell structure is fastened with a set of bolts or by another fastening mechanism.

End plates need to be well designed to have sufficient mechanical strength and stiffness while consisting of a minimum amount of materials. A good design of the PEMFC stack requires that the contact pressure in each cell is not only approximately equal but also has as uniform distribution as possible [5]. In general, there may be high contact electrical resistance at the interface between the gas diffusion layer (GDL) and the bipolar plate (BPP) if the contact pressure is unreasonably small [6–8]. However, the permeability of the GDL will be too low to provide high reaction efficiency if the contact pressure is excessively large [9]. In the practical design of a fuel cell stack system, the end plates are designed to be as rigid as possible so that the clamping load applied by the bolt assembly can be uniformly distributed within the whole fuel cell stack.

From a design point of view, high rigidity of the end plate can be simply achieved by increasing its thickness. However, an end plate that is too thick will provide a too large mass or volume [5]. To achieve low mass and high rigidity simultaneously, end plates with complex configurations, such as ribbed-, bomb-, or bow-shaped end plates [10], have been developed. Although most of these designs seem to be fairly effective, none are based on topology optimization, a powerful theoretical tool for designers to find the best topology or layout for given objectives under specific constraints [11].

In this paper, a multi-objective topology optimization model based on finite element analysis (FEA) is proposed to obtain the optimized material distribution (topology) of the end plate in a specific design space. The optimization objectives are to maximize the stiffness of the end plate and unify the pressure distribution at the contact interfaces of the fuel cell stack at the same time. Combined with the equivalent stiffness model proposed in our previous works [12,13], the optimization design is realized and verified respectively using the commercial software Optistruct® and Abaqus®.

2. Basic theory

2.1. Topology optimization

According to the types of design variables, the optimization design of structures (only continuum structures are considered in

* Corresponding author. Tel.: +86 411 84706353; fax: +86 411 84706353.
E-mail address: cwwu@dlut.edu.cn (C.W. Wu).

0378-7753/$ – see front matter © 2010 Elsevier B.V. All rights reserved.
doi:10.1016/j.jpowsour.2010.08.072

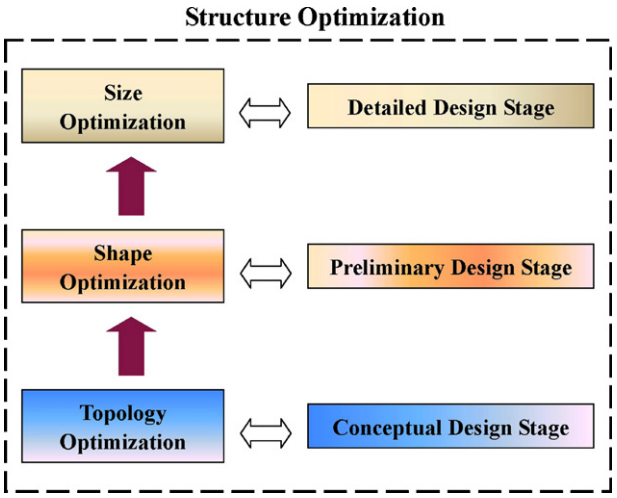

Fig. 1. Schematic diagram of the relationship between the optimization methods and design stages.

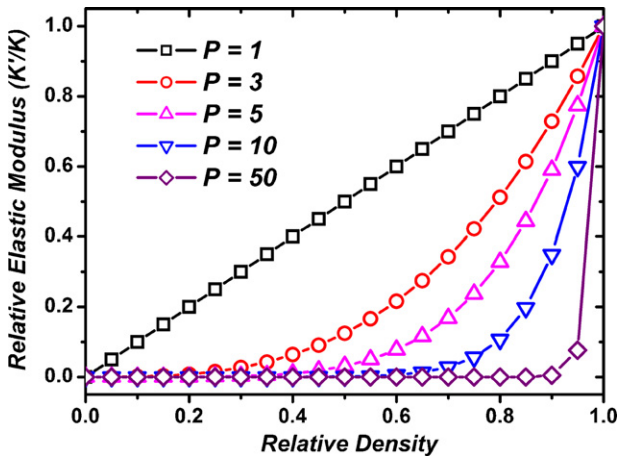

Fig. 2. Schematic diagram of the SIMP method with several penalization factors.

this paper) can be divided into three levels – size, shape and topology optimizations – corresponding to the three stages of the design process [11], as shown in Fig. 1. Topology optimization is carried out at the top level and aims to find the best distribution of material in the specified design space, thus setting the optimized route for load transmittance. The importance of this optimization lies in the fact that the choice of the appropriate topology of a structure in the conceptual design stage is generally the most decisive factor of the product's efficiency. Moreover, size and shape optimizations do not change the structural topology in the process of finding the optimal solution. Therefore, the topology optimization is a valuable tool in preprocessing of the size and shape optimizations [14,15].

Since the homogenous method was first introduced by Bendsøe and Kikuchi [16] in 1988 to solve topology optimization problems of continuum structures, many new methods have been developed, such as the variable density method (VDM), variable thickness method, and evolutionary structural optimization. Among the methods, the VDM is one of the most widely used and is often integrated with FEA. In the VDM, the material density of each element is considered as the design variable and varies continuously between 0 and 1, where "0" represents a "void" and "1" represents the "solid". Intermediate values of the density between 0 and 1 represent fictitious material. Originally, the stiffness of material is assumed to depend linearly on the density. However, this assumption usually causes numerous gray areas in the intermediate density region, which are impracticable when determining the topology of a given material or using different materials within the design space. Hence, a technique is needed to penalize the intermediate densities and force the final design density to be approximately either 0 or 1. In practice, the solid isotropic microstructure with penalty (SIMP) method [17–19] is widely used. It can be expressed for any two-dimensional or three-dimensional solid element as

$$K'(\bar{\rho}) = \bar{\rho}^P \times K, \tag{1}$$

where K' and K are respectively the penalized and real stiffness matrixes of an element, $\bar{\rho}$ is the relative density (a design variable), and P is the penalization factor. The relationship among these parameters is shown in Fig. 2. It is found that the larger the penalization factor, the more discrete the obtained results. Bendsøe and Sigmund [20] showed that good results can be obtained using the SIMP method when $P \geq 3$. In this paper, the SIMP method with $P = 3$ is employed for local topology optimization problems.

2.2. Multi-objective optimization

In a practical optimization problem, there are usually several conflicting design criteria. For example, objectives to reduce the weight and increase the stiffness of a structure cannot simply coexist in one optimization problem since only a single objective can be considered in each optimization process. Consequently, a so-called multi-objective (multi-criteria, vector, Pareto) optimization method has been developed as a methodology for solving optimization problems with several simultaneous objective functions [21].

In general, multiple objectives need to be transformed into a single objective by retaining one selected criterion to be optimized while treating the remaining objectives as either constraints or by assigning suitable weights. However, the choice of constraint limits may be a difficult task because most design quantities do not have a constraint nature. Thus, a norm method with weighting coefficients [21–23] is proposed in this paper.

2.3. Equivalent stiffness model of the PEMFC stack

An equivalent stiffness model of the PEMFC stack has been established by the authors [12,13]. Using this model, the whole fuel cell stack is simplified as a mechanical model consisting of a large number of elastic elements (springs) in either series or parallel. Thus, the stack structures in this paper, except for the end plates, insulator plates, and current collectors, can be reduced to cuboids with specific stiffness to reduce the task of topology optimization. Young's modulus of the cuboids can be calculated using

$$k = \frac{EA}{L}, \tag{2}$$

where k is the equivalent stiffness of the corresponding component [12], E is Young's modulus, A is the cross-section area, and L is the length along the axial direction.

3. Model demonstrations

3.1. Geometry

A three-dimensional FEA model including the insulator plates and current collectors is established on the basis of a previously designed PEMFC stack structure [24] but with the following changes and simplifications:

(a) Parallel flow channel structure is one of the most common structures used in PEMFC stacks owing to its simplicity

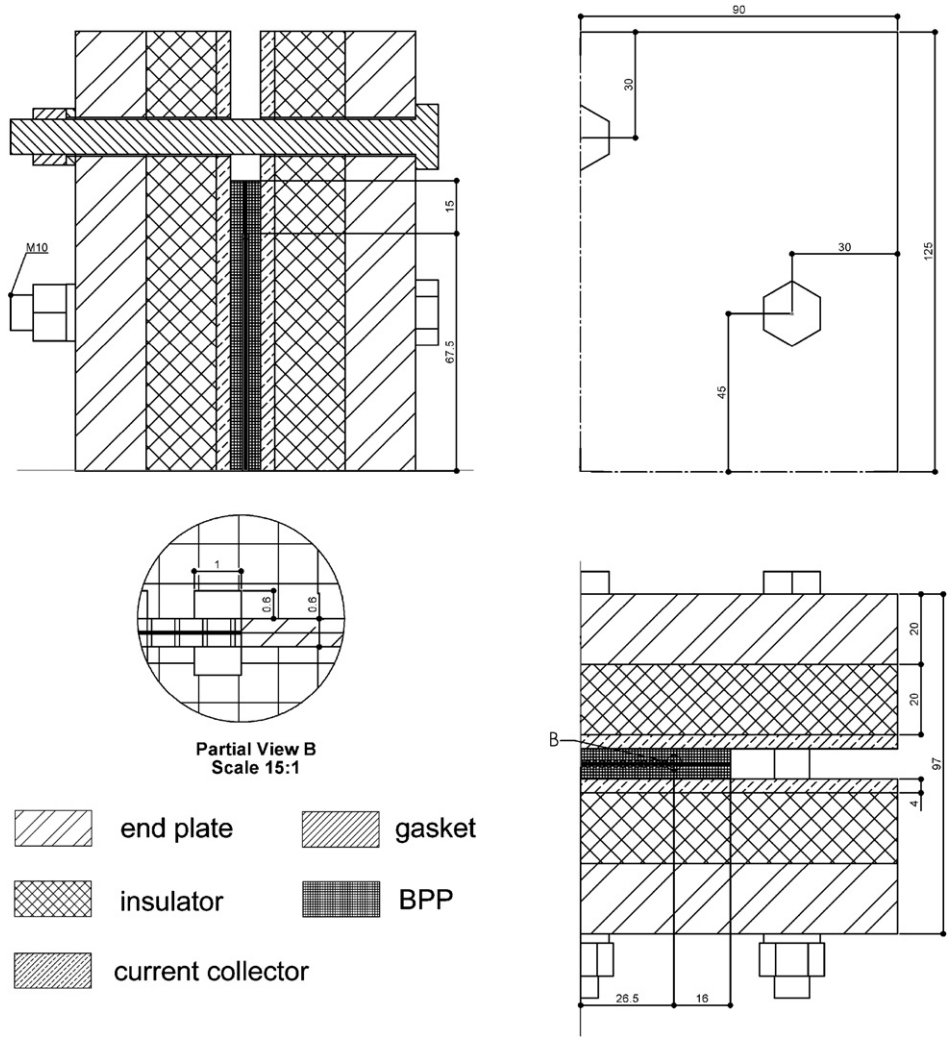

Fig. 3. Dimensions of the single-cell structure.

in design and processing. Therefore, it is adopted in this paper.

(b) Because thermal effect is not taken into account in this paper, existence of the cooling channels might only affect the structural stiffness. However, according to the equivalent stiffness model [12,13], the cooling channel structure with a small cross-section has a minor influence on the structural stiffness. Although any types of the cooling channel structure can be included in our optimization model, the original cooling channels in BPPs will not considered in the present paper for simplicity.

(c) Gasket sealants like ones given in Ref. [25] are adopted because they show roughly a linear mechanical response under clamping load and have been widely used in practical applications.

In the following, the single PEMFC structure with six-bolt assembly similar to that in the previous design [24], as shown in Fig. 3, is studied. Only 1/8 of the single cell is considered owing to structural symmetry. The thicknesses of the PEM and GDL are respectively 0.05 and 0.275 mm [25–27].

3.2. Finite element mesh and material properties

A mapped meshing method is adopted to ensure proper element connectivity and a reasonable aspect ratio. Moreover, there are restrictions to the element size in the design area. Since extremely small features produced in the topology optimization are usually unacceptable in the manufacturing process, a minimum dimension constraint should be introduced in the optimization model. Usually, the mean element size should be less than one-third of the minimum dimension constraint. As the end plates studied here are made of aluminum alloy, the minimum dimension constraint is assumed to be 6 mm according to the corresponding machining process. Therefore, the mean element size for the end plates is chosen to be 2 mm.

Material properties of each component in the stack are listed in Table 1. All components are assumed to have linear elastic behavior.

3.3. Boundary conditions and optimization parameter settings

Symmetry constraints are applied to the symmetrical planes to prevent rigid-body displacements. A contact algorithm is used to simulate the interactions between the two components as shown in Fig. 4. Therefore, highly nonlinear factors are involved in this topology optimization model. The clamping load is calculated from the tightening torque (16 N m) [24] and applied at the corresponding positions of the bolts.

The design area should be specified before setting the optimization model. The material of the end plate far from the clamping bolts is removed as it contributes little to the assembly load bear-

Table 1
Material properties of the stack hardware.

Component	Material	Young's modulus (GPa)	Poisson's ratio	Source
PEM	Nafion®	0.19	0.25	[26]
GDL	Carbon paper	10	0.25	[26]
Bipolar plate	Graphite	10	0.25	[26]
Sealant	VMQ	5.5	0.3	[28]
Current collector	Copper	100	0.33	[29]
Insulation plate	POM	2.6	0.386	[29]
End plate	Aluminum alloy	69	0.33	[29]
Clamping bolt and nut	SS 304	209	0.28	[29]
Washer	Aluminum bronze	110	0.3	[29]

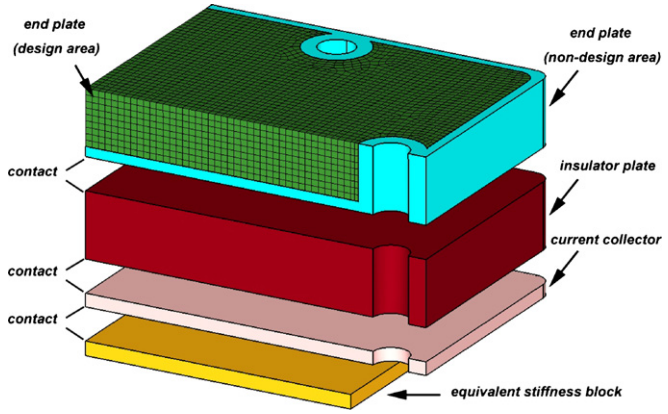

Fig. 4. Schematic diagram of the optimization model. (Only the mesh of the design area is displayed.)

ing. Since the topology optimization is sensitive to the initial design area, which should be as large as possible [11], only regions around the bolt holes, the supported edge and the bottom side are excluded during optimizing (see Fig. 4).

There are two objectives that need to be considered simultaneously: maximizing the structural rigidity of the end plate and uniformizing the pressure distribution in the whole stack. The former can be carried out through minimizing the structural compliance [23] and the latter can be achieved by minimizing the root mean square (RMS) of the displacements at all nodes in the contact area between the current collector and the equivalent stiffness block. Consequently, the multi-objective of the model is formulated as [21–23]

$$\text{minimize}: \left\{\omega_1^q\left[\frac{C(\bar{\rho})-C_{\min}}{C_{\max}-C_{\min}}\right]^q+\omega_2^q\left[\frac{RMS(\bar{\rho})-RMS_{\min}}{RMS_{\max}-RMS_{\min}}\right]^q\right\}^{1/q}, \quad (3)$$

where ω_1 and ω_2 are weighting coefficients, $C(\bar{\rho})$ and $RMS(\bar{\rho})$ respectively are functions of the compliance of the end plate and the root mean square mentioned above, $C_{\max}$ and $RMS_{\max}$ are the corresponding responses determined for the original structure, and $C_{\min}$ and $RMS_{\min}$ are calculated by solving the single-objective optimization problems expressed as

$$\text{minimize}: C(\bar{\rho}), \quad (4)$$

and

$$\text{minimize}: RMS(\bar{\rho}). \quad (5)$$

Here, $\omega_1 = \omega_2 = 0.5$ and $q = 0.5$ are chosen for this problem. The constraint of this optimization model can be written as

$$\text{Volume fraction} = \frac{\bar{V}-V_{\text{non-design}}}{V_{\text{design}}} \le 0.3, \quad (6)$$

where $\bar{V}$ is the total volume of the whole model in the current iteration, $V_{\text{non-design}}$ is the initial non-design volume, and V_{design} is the initial design volume. The objective is compiled in FORTRAN language as user-defined external functions. The model built here is referred to as the reference optimization model in the following.

4. Optimization results

Results of the topology optimization are usually expressed by the relative density of each element. Therefore, the elements with low densities are hidden to provide clear guidance for the establishment of the optimized topology of the structure. In the following figures, the color difference expresses the morphology of end plate. If the single-objective optimization method is used, to increase the rigidity of the end plate, material should be concentrated in the area linking the two adjacent bolt holes, as shown in Fig. 5(a). However, this will definitely increase elastic deformation in the center of the end plate, and thus, the contact pressure in the GDLs will be terribly non-uniform. On the other hand, to obtain a pressure distribution as uniform as possible at the contact interfaces, it is effective to stiffen the structure in the contact area as depicted in Fig. 5(b). Yet in this case, there may be large deformation and unreasonable stress concentration

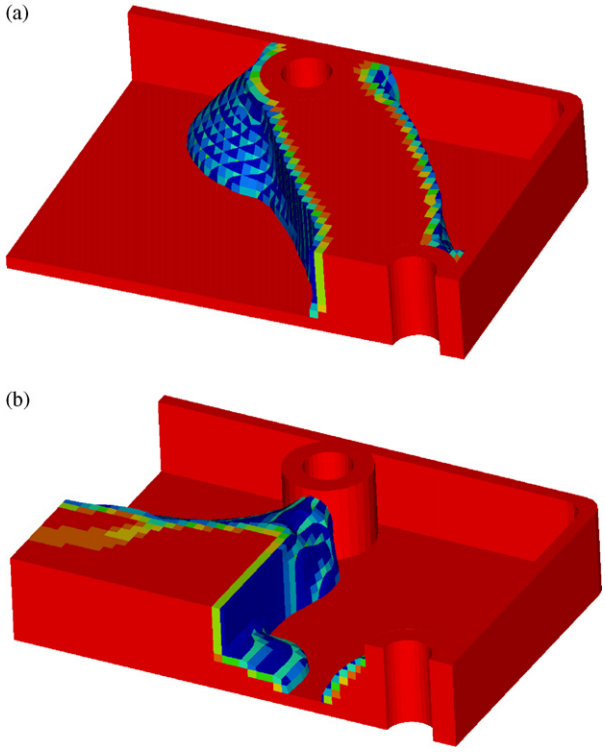

Fig. 5. Schematic diagram of the single-objective optimization designs: (a) minimizing the structural compliance and (b) minimizing the RMS of the displacements at all nodes in the corresponding contact area. Elements displayed here (and hereinafter) have relative densities greater than 0.3.

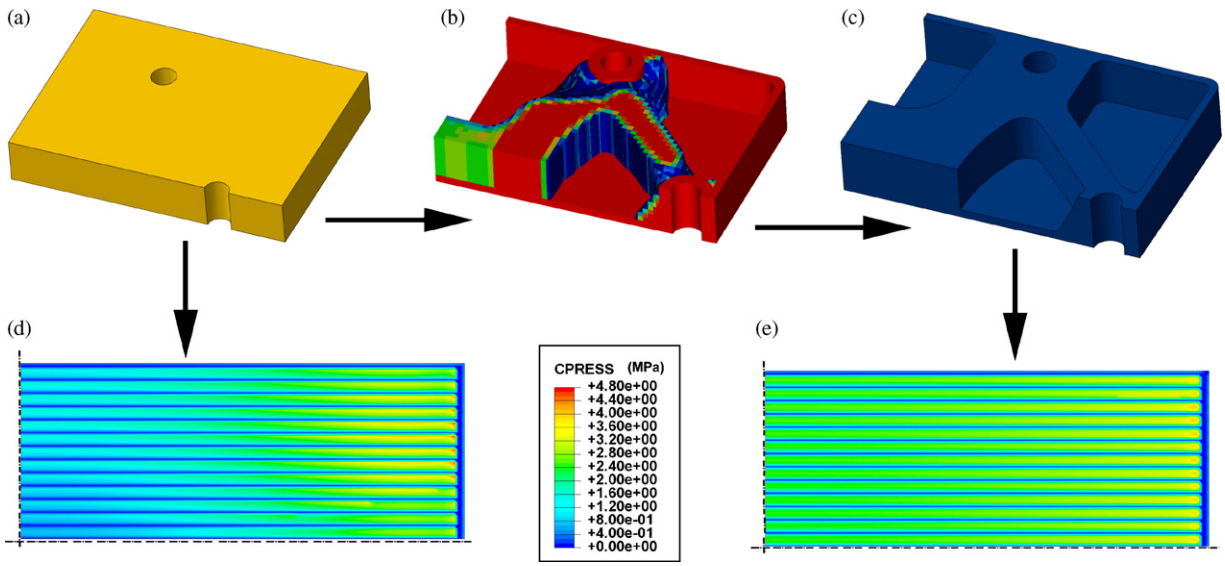

Fig. 6. Schematic diagram of the multi-objective optimization design: (a) original end plate; (b) optimization result; (c) manufacturing design according to the optimization result; (d) contact pressure distribution on the GDL for the original structure; (e) contact pressure distribution on the GDL for the optimized structure.

in the end plate, which are obviously against the design purpose.

Fig. 6 shows the detailed multi-objective optimization process for the end plate. Fig. 6(a) is the original end plate. Fig. 6(b) shows the optimized topology considering the multi-objective, which can be approximately regarded as the combination of results depicted in Fig. 5(a) and (b). A new geometry of the end plate is obtained (see Fig. 6(c)) according to the material distribution given in Fig. 6(b). The optimized structure is validated using nonlinear contact FEA models established in Abaqus®. It is found that when the fuel cell stack is equipped with the original end plate, the contact pressure at the center of the GDL is much less than that at the edge, as shown in Fig. 6(d). Hence, the pressure distribution on the contact surface between the GDL and BPP is obviously non-uniform, which may induce an increase in the interfacial ohmic resistance in the center region. On the other hand, if the optimized structure is used instead, the contact pressure distribution over the whole cell area is very much improved (Fig. 6(e)). Hence, the contact pressure with optimization is much better than that without. Moreover, the volume of the optimized end plate as shown in Fig. 6(c) is reduced

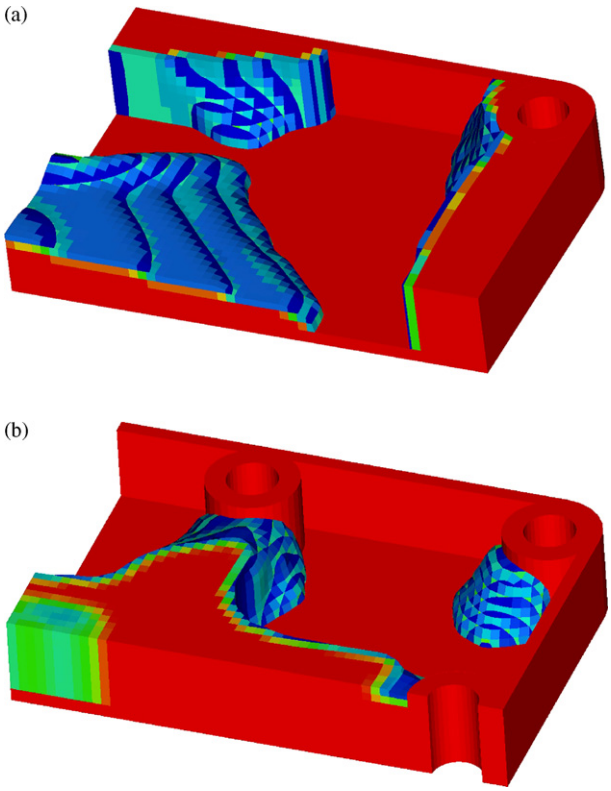

Fig. 7. Schematic diagram of the multi-objective optimization designs for different numbers of clamping bolts: (a) 4 clamping bolts and (b) 10 clamping bolts.

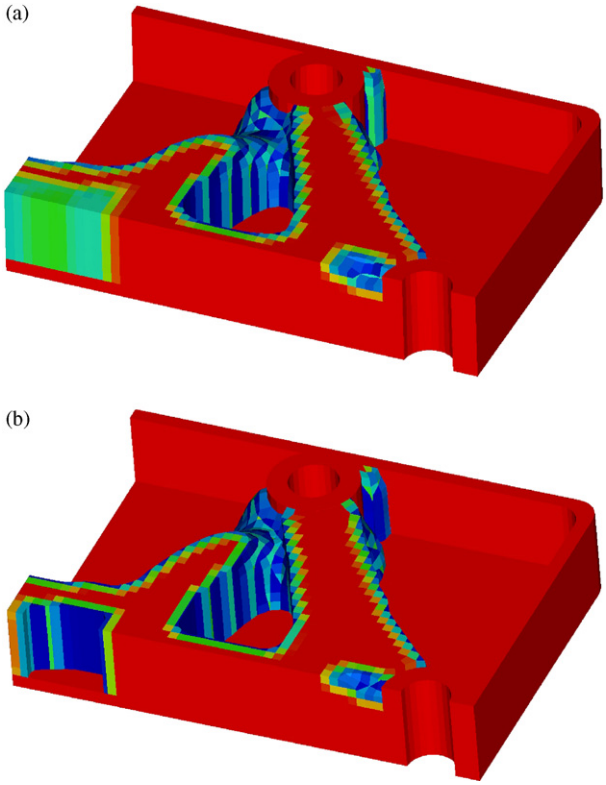

Fig. 8. Schematic diagram of the multi-objective optimization designs for different numbers of cells (six-bolt assembly): (a) 5-cell stack and (b) 10-cell stack.

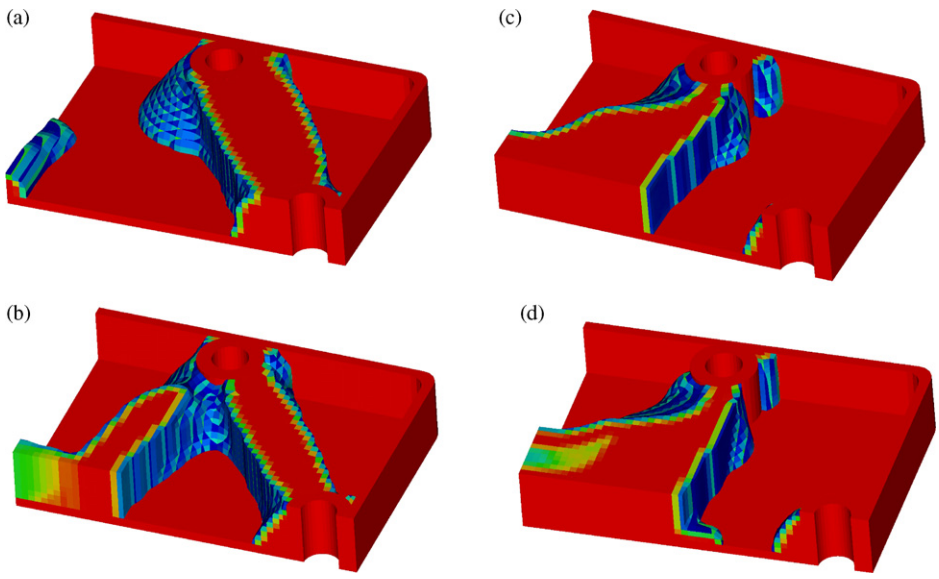

Fig. 9. Schematic diagram of the multi-objective optimization designs for several combinations of weighting coefficients: (a) $\omega_1 = 0.7$, $\omega_2 = 0.3$; (b) $\omega_1 = 0.6$, $\omega_2 = 0.4$; (c) $\omega_1 = 0.4$, $\omega_2 = 0.6$; (d) $\omega_1 = 0.3$, $\omega_2 = 0.7$.

to one-third of that of the original structure. However, it should be noted that although the results of topology optimization provide good guidance for better material distribution, they cannot be regarded as fully optimized structures.

5. Discussions

There are too many types of PEMFC stack products to list. It is impossible to completely consider all the variable features at once owing to their numerous possible combinations. In this paper, several common cases are considered to illustrate the influences of design parameters on the optimization results.

5.1. Effect of the number of clamping bolts

Here, two additional types of end plate structures (Fig. 7), containing 4 and 10 bolts respectively, are studied. Although the optimized structures in Fig. 7(a) and (b) are distinct, there are still some design rules available. For example, to keep the contact pressure as uniform as possible, the end plates should be strengthened in the area of possible large deformation, thus increasing the local stiffness.

5.2. Effect of the number of cells

Taking advantage of the equivalent stiffness model described in the literature [12,13], equivalent stiffness versus the number of cells can be rapidly calculated. According to Fig. 8(a) and (b), the optimized material distributions vary with the number of cells. This is mainly because the contact response changes as the equivalent stiffness of the stack decreases nonlinearly with an increase in the number of cells [13]. However, the optimized material distributions remain similar.

5.3. Multi-objective optimization with different weighting coefficients

The two weighting coefficients are both 0.5 in the reference optimization model, indicating that they make the same contribution to the final objective. In a practical design, the two coefficients need to be adjusted in accordance with the requirements of different problems. For example, if the above design is inclined to the first single-objective optimization, the first corresponding weighting coefficient should be increased appropriately. Here, topology optimizations for another four groups of combinations of the weighting coefficients are studied, as shown in Fig. 9. Comparing with Fig. 5, it is seen that when a weighting coefficient is increased, the obtained topology of the structure is closer to its corresponding single-objective optimization. However, it cannot be simply assumed that a similar combination of the coefficients always leads to similar optimized topology owing to the nonlinearity of Eq. (3). Therefore, there are two entirely different topologies as depicted in Fig. 9(b) and (c). In most circumstances, several trials are needed for engineers to obtain the best combination of weighting coefficients.

6. Conclusions

In this paper, a multi-objective topology optimization model of the end plate in a PEMFC with nonlinear contact boundary conditions has been established to obtain the optimized material distribution, and as a result, maximize the stiffness of the end plate and make the pressure distribution uniform across the whole cell. It is found that the structure designed according to the topology optimization will meet both the requirements of low weight and manufacturability. The topology optimization is the basis for the shape optimization and size optimization of end plates and could provide good guidance for designers to obtain a better material distribution at the early design stage.

Acknowledgment

This work was supported by the National Natural Science Foundation of China (10972050, 90816025, 10721062).

References

[1] R.V. Helmolt, U. Eberle, J. Power Sources 165 (2007) 833–843.
[2] A. Kundu, J.H. Jang, J.H. Gil, C.R. Jung, H.R. Lee, S.H. Kim, B. Ku, Y.S. Oh, J. Power Sources 170 (2007) 67–78.
[3] A.S. Patil, T.G. Dubois, N. Sifer, E. Bostic, K. Gardner, M. Quah, C. Bolton, J. Power Sources 136 (2004) 220–225.
[4] M. Uzunoglu, O.C. Onar, M.S. Alam, J. Power Sources 168 (2007) 240–250.
[5] S. Karvonen, T. Hottinen, J. Ihonen, H. Uusalo, ASME J. Fuel Cell Sci. Technol. 5 (2008) 1–9.

[6] P. Zhou, C.W. Wu, G.J. Ma, J. Power Sources 159 (2006) 1115–1122.
[7] P. Zhou, C.W. Wu, G.J. Ma, J. Power Sources 163 (2007) 874–881.
[8] P. Zhou, C.W. Wu, J. Power Sources 170 (2007) 93–100.
[9] L. Cinderlla, A.M. Kannan, J.F. Lin, K. Saminathan, Y. Ho, C.W. Lin, J. Wertz, J. Power Sources 194 (2009) 146–160.
[10] J. Evertz, M. Günthart, Int. Conf. with Exhibition in 2nd European PEFC Forum, 2003, pp. 469–482.
[11] H.A Eschenauer, N. Olhoff, Appl. Mech. Rev. 54 (2001) 331–390.
[12] P. Lin, P. Zhou, C.W. Wu, J. Power Sources 194 (2009) 381–390.
[13] P. Lin, P. Zhou, C.W. Wu, J. Power Sources 195 (2010) 1383–1392.
[14] M. Bremicker, N. Kikuchi, M. Chirehdast, P.Y. Papalambros, Mech. Struct. Mach. 19 (1991) 551–587.
[15] N. Olhoff, M.P. Bendsøe, J. Rasmussen, Comp. Meth. Appl. Mech. Eng. 89 (1991) 259–279.
[16] M.P. Bendsøe, N. Kikuchi, Comp. Meth. Appl. Mech. Eng. 71 (1988) 197–224.
[17] M.P. Bendsøe, Struct. Optim. 1 (1989) 193–202.
[18] M. Zhou, G.I.N. Rozvany, Comp. Meth. Appl. Mech. Eng. 89 (1991) 309–336.
[19] G.I.N. Rozvany, M. Zhou, T. Birker, Struct. Optim. 4 (1992) 250–252.
[20] M.P. Bendsøe, O. Sigmund, Arch. Appl. Mech. 69 (1999) 635–654.
[21] S. Min, S. Nishiwaki, N. Kikuchi, Comp. Struct. 75 (2000) 93–116.
[22] J. Koski, R. Silvennoninen, Int. J. Numer. Meth. Eng. 24 (1987) 1101–1121.
[23] T.Y. Chen, S.C. Wu, Comp. Mech. 21 (1998) 483–492.
[24] C.Y. Wen, Y.S. Lin, C.H. Lu, J. Power Sources 192 (2009) 475–485.
[25] D. Bograchev, M. Gueguen, J.C. Grandidier, S. Martemianov, J. Power Sources 180 (2008) 393–401.
[26] A. Kusoglu, A.M. Karlsson, M.H. Santare, S. Cleghorn, W.B. Johnson, J. Power Sources 161 (2006) 987–996.
[27] Y. Tang, M.H. Santare, A.M. Karlsson, S. Cleghorn, W.B. Johnson, J. Fuel Cell Sci. Technol. 3 (2006) 119–124.
[28] S.J. Lee, C.D. Hsu, C.H. Huang, J. Power Sources 145 (2005) 353–361.
[29] http://www.engineeringtoolbox.com/.